Journal of Petroleum Science and Engineering 219 (2022) 111055

Contents lists available at ScienceDirect

Journal of Petroleum Science and Engineering

journal homepage: www.elsevier.com/locate/petrol

Triaxial behavior of a stabilized and a highly porous oil well cement paste at different saturation and drainage conditions

Victor Nogueira Lima [a], Hans Joakim Skadsem [b,c,*], Katherine Beltrán-Jiménez [c], Alexandr Zhemchuzhnikov [a], Raquel Quadros Velloso [a], Flávio de Andrade Silva [a]

[a] Department of Civil and Environmental Engineering, Pontifícia Universidade Católica do Rio de Janeiro (PUC-Rio), Rua Marquês de São Vicente 225, 22451-900 Rio de Janeiro, Brazil
[b] University of Stavanger, P.O. Box 8600, 4036 Stavanger, Norway
[c] Norwegian Research Centre AS, P.O. Box 8046, 4068 Stavanger, Norway

ARTICLE INFO

Keywords:
Cement
Zonal isolation
Triaxial testing
Porosity
Permeability
Saturation
Drainage

ABSTRACT

Well cement is the most common barrier material in wells for geothermal and hydrocarbon production. As cements are exposed to hydrostatic loads and periods of deviatoric loading in wellbore environments, it is important to understand the mechanical behavior of cement under relevant conditions. We study effects of porosity, saturation, confining pressure and drainage conditions on the mechanical behavior of class G well cement using two basic formulations, one which produces a highly porous cement paste. The high-porosity cement exhibited lower strength and reduced elastic moduli compared to the stabilized formulation. The elastic moduli for both formulations were reduced with increasing confining pressure, and the most pronounced effect of confinement was increased ductility and pronounced strain hardening behavior of the two cements, likely due to compaction. Under saturated and undrained conditions, the stabilized cement exhibited an increase in stiffness and essentially brittle failure even at 20 MPa confining pressure. The porous cement showed less sensitivity to drainage conditions. We attribute this observation to possible generation of internal micro-cracks and dislocations instead of a macroscopic failure plane. The results contribute to increased understanding of the mechanical response of conventional and porous cements under relevant confining pressures and different saturation and drainage conditions.

1. Introduction

Oil well cement paste is by far the most widely used material for zonal isolation in wells for hydrocarbon or geothermal energy recovery, or for geological sequestration of carbon dioxide. Cement is used both for isolating the annular space behind casing strings, for sealing fractures and for plugging and abandoning mature wells, (Nelson and Guillot, 2006). A conventional oil well cement slurry is typically mixed with approximately 44% water to the weight of cement, and can contain a number of additives to achieve the desired properties and slurry stability. Once placed in the well, the cement slurry will gradually transform to a hardened cement paste, that consists mainly of calcium silicate hydrates (C-S-H) and calcium hydroxide (CH), from the C_3S and C_2S hydration reactions, possibly unreacted cement particles and pores ranging from nanometer-sized gel pores to micron-sized capillary pores, (Jennings et al., 2002). The calcium silicate hydrates account for approximately 75% of the hardened cement paste, and are essentially colloidal gels that contain water-filled gel pores as well as chemically bound water. The larger capillary pores are formed in the presence of excess water, and reside in the space not occupied by the porous gel phase, (Jennings et al., 2002). Larger pores or voids may also be present in the cement paste as a result entrained air during the mixing process. The porosity of the hardened cement paste is a result of the water/cement ratio used when mixing the cement: depending on the type of Portland cement used, the minimum water/cement ratio for complete hydration is considered to range from 0.39 to 0.44 (Taylor, 1997; Jennings et al., 2002; Brouwers, 2004); less mixing water will hinder the hydration process due to insufficient space for its products, and more mixing water will generate excess capillary porosity.

As well cement is a main barrier element and responsible for zonal isolation and well integrity, it is necessary to understand the mechanical behavior and strength of cement under relevant downhole conditions, including confining pressure and thermal and mechanical stresses (Bois et al., 2011). Oil well cement pastes normally exhibit an initial linear elastic response to applied stresses, with a Young's

* Corresponding author at: University of Stavanger, P.O. Box 8600, 4036 Stavanger, Norway.
E-mail address: hans.j.skadsem@uis.no (H.J. Skadsem).

https://doi.org/10.1016/j.petrol.2022.111055
Received 11 April 2022; Received in revised form 2 September 2022; Accepted 11 September 2022
Available online 15 September 2022

modulus of the order of 10 GPa, and a brittle failure at an unconfined compressive strength in the range of 30 to 60 MPa, depending on the composition and age of the cement. A confining pressure has been shown to induce considerable ductility and a certain frictional strengthening of cement pastes, and also to prevent failure and the loss of load-carrying capability (Handin, 1965; Nelson and Guillot, 2006). Furthermore, it has been shown by Ulm et al. (2004) and Ghabezloo et al. (2008) that the mechanical behavior of cement pastes can be described within the framework of poromechanics, *i.e.* using effective stresses and effective stress coefficients from an appropriate porosity value (Ghabezloo et al., 2008). A direct consequence of this behavior is a sensitivity to drainage conditions during mechanical testing with confining pressure for certain weakened cements (*e.g.* calcium-leached cements) (Heukamp et al., 2001, 2003; Yurtdas et al., 2011).

As pointed out above, hardened cement paste is a porous material with gel pores, chemically bound water and larger capillary pores, and this porosity affects the mechanical behavior of cements. In oil well cementing, entrained air at the rig site during batch mixing or gas migration from open-hole formations can result in an increased bulk cement porosity. In some cases, gas is intentionally introduced into the cement slurry to reduce its density and produce a foamed cement slurry. Reducing the mass density of the slurry by injecting gas allows cementing across weaker formations where the fracture pressure is low. Foamed cements are often prepared by adding a surfactant and stabilizing agents to the base cement slurry, and injecting nitrogen gas into the slurry as it is being pumped into the well, (Nelson and Guillot, 2006). Introduction of gas can reduce the density of the slurry considerably (de Roziéres and Ferriére, 1991), but will also impart a considerable porosity (often $> 40\%$, depending on the entrained gas fraction, Cunningham et al., 2017).

The measurement of cement paste porosity is not always trivial and different methods can produce quite variable results, as pointed out by Krus et al. (1997). In general, Krus et al. (1997) noticed that mercury intrusion porosimetry and helium pycnometer porosimetry are corresponding for almost all samples evaluated, except for specimens with a large number of micropores, such as cement paste with slag addition. In the same way, Hedenblad (1997) found a good agreement between the mercury intrusion porosimetry and helium porosimetry for most of the cement paste specimens tested. However, he also stated an influence of the porosity and permeability on the porosimetry technique. For Hedenblad (1997) and Krus et al. (1997), the sample with the addition of slag showed lower porosity in the mercury intrusion porosimetry technique because slag additions provide a considerable decrease in the permeability, decreasing the average diameter of the pores, which makes the procedure of porosimetry by mercury intrusion difficult, since it has a limitation to voids of 0.4 nm in diameter (Pavía and Condren, 2008; Rashad, 2018; Irico et al., 2021; Ahmed, 2022).

As with most porous materials, the strength of cement pastes is affected by its porosity, since the load-carrying capacity is provided by the solid material, (Yudenfreund et al., 1972). An increase in the porosity of cement paste, for instance by mixing excess water or gas into the slurry, will normally result in a decrease in the bulk modulus of the material and compaction or pore collapse under high mean stress levels. Different empirical models relating porosity ϕ and strength σ has been proposed, including a linear correlation, a polynomial, an exponential or logarithmic correlation (Table 1). These correlations are expressed in terms of a parameter α_i, and (for the logarithmic correlation) the zero strength porosity of the material, and have been shown to provide good agreement for the compressive strength over a range of porosities, (Roy and Gouda, 1973; Chindaprasirt et al., 2008).

The models mentioned above connect the material strength mainly to the porosity of the sample. Observations reported by Mindess (1970), Kendall et al. (1983) and Odler and Rößler (1985) suggested that the pore size also could affect the strength; cement pastes made by different processes could exhibit a relative strength difference by as much as 60%, even if the total porosity was approximately the same

Table 1
Summary of equations that correlate porosity and material strength.

Equation	Reference
$\sigma^* \sim 1 - \alpha_1 \phi$	Hasselman (1963)
$\sigma^* \sim (1 - \phi)^{\alpha_2}$	Balshin (1949)
$\sigma^* \sim \exp(-\alpha_3 \phi)$	Ryshkewitch (1953)
$\sigma^* \sim \ln(\phi_0/\phi)$	Schiller (1971)

across samples (Kendall et al., 1983). This observation was attributed to the existence of larger, millimeter-sized crack-like pores in the weaker cement pastes. These macro-defects, which were traced back to the mixing process and the existence of entrained air bubbles and voids in the cement slurry, are more prone to initiate fractures through the material than the smaller gel pores or capillary voids. Odler and Rößler (1985) found that the porosity due to gel pores with radii smaller than 10 nm did not significantly affect the strength of a cement paste, and that the larger pores are more significant in terms of weakening the cement. As discussed by Kendall et al. (1983), the effect of pore size on material strength can be captured by the Griffith model of fracture in brittle materials (Griffith, 1921), where the fracture stress (σ) is related to the elastic modulus (E), the fracture surface energy (γ) and the size of the flaw (a). Assuming the porosity-dependence $E = E_0(1 - \phi)^3$ and $\gamma = \gamma_0 \exp(-k\phi)$ with E_0 and γ_0 the elastic modulus and fracture surface energy at $\phi = 0$, and k a model constant, Kendall et al. (1983) proposed the strength criterion $\sigma = [E_0\gamma_0(1 - \phi)^3 \exp(-k\phi)/(\pi a)]^{1/2}$, where the strength is seen to scale as $\sigma \sim a^{-1/2}$. Thus, the model suggests that the presence of a few large voids can significantly deteriorate its strength, (Kendall et al., 1983). A modified version of this model was used by Lian et al. (2011), who found strong correlations between strength measurements and the calibrated crack model. Thus, and as pointed out by Taylor (1997), these observations suggest that it is more appropriate to correlate the mechanical strength of cement paste to the capillary porosity rather than the total porosity, (Taylor, 1997).

In most of the analytical models, the pores are considered spherical or approximately spherical, resulting in purely isotropic damage, (Contrafatto et al., 2016). Furthermore, He et al. (2022) states that secondary damage can occur due to the formation of deformation-induced microcracks in the vicinity of the pore. According to Fassin et al. (2019), the strength of the material will be directly influenced by the microcracks due to the appearance and development of anisotropic damage. Therefore, some researchers define cementitious material as a multiphase material for damage analysis, since both pores and microcracks can influence the material damage process, (Liu et al., 2018). Moreover, according to He et al. (2022), the confining pressure also affects the cement paste damage depending on the porosity. For low confining pressures, the pores are prone to develop tensile stresses in the direction parallel to the loading application, leading to crack propagation due to the low tensile strength of cementitious materials. On the other hand, when subjected to high confining pressures, the pores undergo compaction, which makes it difficult for cracks to appear and propagate, (He et al., 2022).

More recent studies have explored the combined effects of porosity, saturation and confining pressure on the mechanical behavior of concretes. Vu et al. (2015) considered the impacts of saturation on the triaxial stress–strain behavior of a high-performance concrete with a water/cement ratio of 0.44 and a porosity (available to water) of 12%. Tests on dry samples with saturation of approximately 60% showed an increase in stiffness and strength with increasing confining pressure, an effect that was attributed to pore collapse and compaction (Vu et al., 2015). Measurements performed with dry and with completely saturated samples at moderate confining pressures (50 MPa) indicated only minor differences in the deviatoric stress–strain behavior. Beyond a mean stress of approximately 100 MPa, the fully saturated samples displayed less volumetric deformation than the dry samples at the same mean stress level, but also a reduced deviatoric strength (Vu et al.,

2015). These observations suggest that at sufficiently high confining pressures, a fully saturated sample (with completely water-filled pores) will have a larger effective bulk modulus than a dry or partially saturated sample, resulting in less volumetric deformation. At the same time, water may lubricate or reduce the effective confining stresses, resulting in a lower shear strength (Vu et al., 2015).

Zingg et al. (2016) examined the influence of capillary porosity and macro-defects due to entrained air on the triaxial behavior of concretes. A high-performance concrete (HPC) was prepared using a relatively low water/cement ratio (0.3) and by adding silica fume to ensure small capillary porosity. A low-performance concrete (LPC) was mixed with considerably more water (water/cement ratio of 0.64) and an air-entraining ingredient in order to increase concentration of macro-defects. The aggregate skeleton was the same for all formulations tested (Zingg et al., 2016). At relatively low confining pressures (50 MPa), the HPC was found to have a higher Young's modulus and a larger ultimate deviatoric stress than the LPC formulation. At considerably larger confining pressures (600 MPa), the concrete samples exhibited very similar stress–strain responses and nearly no sensitivity to initial porosity. These results suggest that considerable mean stresses damage the cement matrix, and that mechanical behavior is then determined largely by the granular skeleton of the concrete and not the initial porosity (Zingg et al., 2016).

Effects of saturation on triaxial concrete behavior was further assessed by Malecot et al. (2019), who utilized HPC and LPC formulations similar to Zingg et al. (2016). In agreement with the study by Vu et al. (2015), also HPC and LPC formulations exhibited minor or insignificant effects of saturation at low-to-moderate confining pressures. The more porous LPC and ordinary concrete (OC) samples exhibited a sensitivity to the saturation at lower mean stress levels and confining pressures compared to the HPC samples, which can be correlated to the larger capillary porosity of LPC and OC (Malecot et al., 2019).

The purpose of the current study is to explore how cement paste porosity affects the triaxial behavior of a conventional oil well cement, and whether the samples are sensitive to drainage conditions, as seen previously in chemically degraded cements (Heukamp et al., 2001, 2003; Yurtdas et al., 2011).

2. Cement paste formulations and test program

As detailed below, two different cement paste formulations have been used in this study to investigate the effects of porosity and saturation on the triaxial behavior of well cement paste: A *stabilized* and a *porous* cement paste. Both formulations are based on class G cement and de-ionized water to a 0.44 water/cement ratio by weight, and a fluid loss additive. The *stabilized* formulation also contains a defoamer additive to control the surfactant characteristic of the fluid loss additive. A defoamer was not used in the *porous* cement paste formulation, which resulted in a significantly higher porosity, as will be detailed below.

A standard oil well cement with mineralogical composition shown in Table 2 was used in this study. The cement had a Blaine fineness of 2788 cm^2/g and a mass density of 3.19 g/cm^3.

The quality of the cement in the absence of additives was tested in accordance with API 10A (API, 2011) and API 10B (API, 2013) by preparing slurries with a water/cement ratio of 0.44 using de-ionized water. The test results were all in accordance with the standard specifications, as summarized in Table 3.

The two additional additives used in this study was a polyvinyl alcohol (PVOH) fluid loss additive with viscosity 49 mPa s, a degree of hydrolysis of 88%, and granulometry between 0.063 mm and 0.25 mm, as shown in Fig. 1. A commercial additive based on fatty alcohol alkoxylate from BASF was used as defoamer. Fatty alcohols are generally derived from natural oils and are proven foam suppressants for a variety of applications in the oil and gas industry (Hewlett, 2003).

Table 2
Chemical composition of Lafarge Holcim Class G oil well cement. Standard refer to API 10A (1) and ASTM C114 (2).

Chemical property	Value	Requirement	Standard
SiO_2, %	22.30	N/A	1, 2
Al_2O_3, %	3.88	N/A	1, 2
Fe_2O_3, %	4.52	N/A	1, 2
SO_3, %	2.37	<3%	1
CaO, %	64.54	N/A	1, 2
MgO, %	1.36	<6%	1
Na_2O, %	0.53	<0.75%	1
K_2O, %	0.36	N/A	1, 2
Loss of ignition, %	0.96	<3%	1
C_3S, %	54	48%–65%	1
C_3A, %	2.6	<3%	1
C_4AF, %	14	N/A	1, 2
$C_4AF + 2C_3A$, %	19	<24%	1

Table 3
Cement quality test results for class G cement paste according to API 10 A specification.

API 10A test	Value	Requirement
Water/cement ratio	0.44	0.44
Free water	4.52%	<5.90%
UCS, cured at 38 °C	4.7 MPa	>2.1 MPa
UCS, cured at 60 °C	13.8 MPa	>10.3 MPa
Thickening time, 30 Bc	71 min	>30 min
Thickening time, 70 Bc	95 min	
Thickening time, 100 Bc	103 min	90–120 min

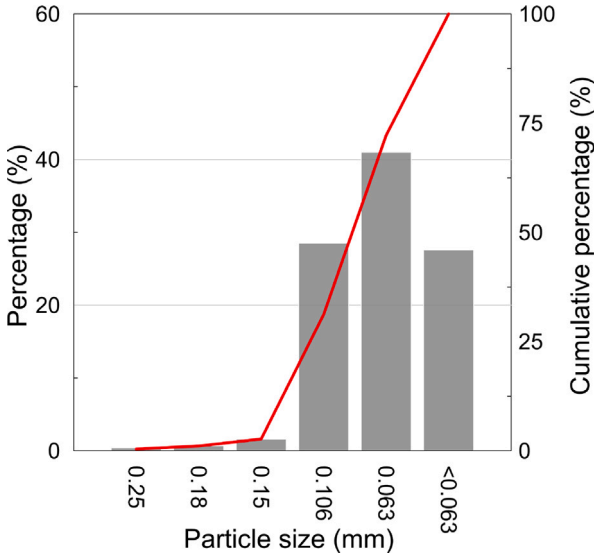

Fig. 1. Particle size distribution for polyvinyl alcohol fluid loss additive.

Table 4
Class G cement paste mixture compositions.

Material	Manufacturer	Mix proportion
Class G cement	Lafarge Holcim	0.44 w/c ratio
Deionized water	–	
Fluid loss additive	Kuraray	0.4% bwoc[a]
Deforamer[b]	BASF	0.1% bwoc

[a]bwoc: By weight of cement.
[b]Only used in the stabilized formulation.

The final composition of the mixtures used in this research is shown in Table 4.

The cement pastes were mixed following the API standard (API, 2013), taking into account the mixing order and using a constant speed

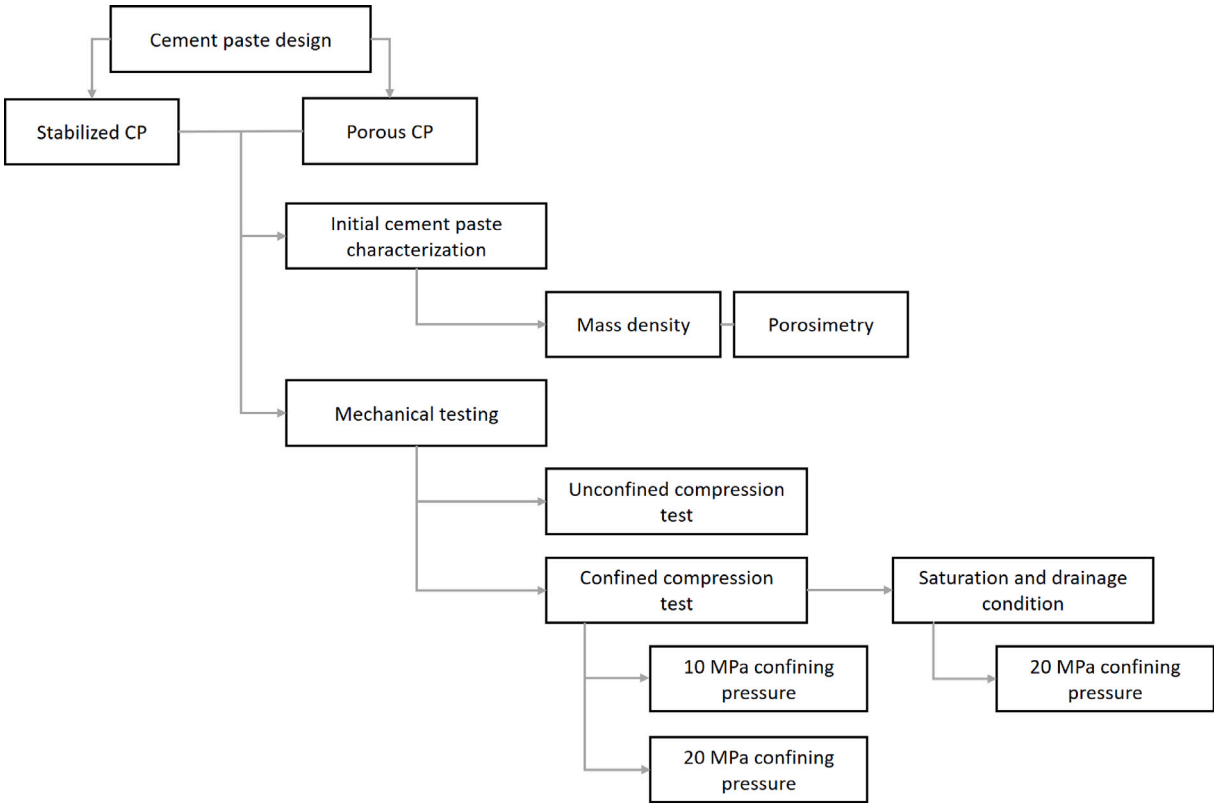

Fig. 2. Experimental program summarized in flowchart.

mixer produced by Chandler model 3260. Mixing was performed with the following steps: (i) Addition of water and liquid additives to the mixing container; (ii) separate manually mixing of cement and powder additives; (iii) adding the dry mixture to the mixing container while mixing at a constant speed of 4000 revolutions per minute (RPM) for 15 s; (iv) mix for another 35 s at a constant speed of 12,000 RPM.

All samples were cured submerged in water for 14 days before mechanical testing. On the fourteenth day, the specimens were removed from the water and taken to smooth the surface, in order to maintain the parallelism between the upper face and the lower face. The unsaturated samples were then taken to the desiccator and left to dry under a pressure of 760 torrs. In the case of saturated tests, the specimens were again submerged in water and taken to a vacuum chamber with a maximum pressure equal to that of the desiccator, to accelerate the saturation process. On the fifteenth day, the mechanical tests commenced.

The experimental characterization and testing of the stabilized and porous cement pastes include mass density measurement, porosimetry, permeability, measurement of unconfined compressive strength and a suite of confined compression tests, covering different confining pressures and saturation conditions. An overview of the test program is provided in Fig. 2.

3. Initial cement paste characterization

A FANN pressurized mud balance was used to measure the mass density of the two cement paste samples used in this study. The stabilized cement paste (with defoamer) had a mass density of 1.9 g/cm^3 while the porous cement paste had a mass density of 1.74 g/cm^3, suggesting a larger porosity than the stabilized cement paste.

Porosity was measured by both helium expansion and by mercury intrusion. The former method allows measuring sample grain and pore volumes, while the latter provides pore size distribution. At first, Corelab Ultrapore 300 helium expansion porosimeter was used. Two 38 mm (1.5 inch) diameter and 70 mm in height samples of each cement paste formulation were made specifically for these tests. In an attempt to eliminate all moisture, which can interfere with the measurement results, the specimens were dried in an oven at 60 °C for 24 h. Cracks that may have been caused by expansion of trapped water were observed in the stabilized cement paste samples. New samples were made, and this time dried in a desiccator with the application of 760 torr vacuum for 24 h.

The helium expansion system can be used in either a grain volume measurement mode, by placing material in a cup with known volume, or in pore volume measurement mode, by connecting a core holder. At least three grain volume measurements were made for each specimen. The low permeability of the cement samples prevented the determination of pore volume. Thus, caliper measurements were used to calculate the porosity using grain volume and total sample volume.

Mercury intrusion tests were performed using AutoPore IV Model 9510. The system can apply pressure up to 414 MPa, which allows measuring pore diameters ranging from 3 nm to 360 μm by filling the chamber containing the sample with mercury. For mercury intrusion porosimetry, one 8 mm cubic sample of each cement paste formulation was prepared. As these tests were outsourced to another laboratory, a standard procedure of oven drying material at 105 °C for 24 h was followed, which may have induced cracks as mentioned earlier. As the porous cement paste contained millimeter sized pores, larger than the maximum size limit, the apparent total volume measured is smaller than what it was found for the gas porosimetry. Moreover, the heating process used for the mercury intrusion porosimetry may have induced cracks that connected isolated pores, and may therefore have resulted in a high apparent porosity for the stabilized cement paste.

Permeability tests were performed using the Corelab Ultra-Perm 610 gas permeameter with nitrogen gas. This equipment is a steady-state gas permeameter for samples of similar size to those previously defined for the helium expansion porosimeter. Overall, this permeameter utilizes an accurate flow measurement process with a set of differential

Table 5
Summary of porosimetry test data from dry weight and specimen volume to grain density and pore volume.

Measurement	Stabilized CP	Porous CP
Porosity, helium expansion (%)	7.1	41.3
Porosity, mercury intrusion (%)	20.3	37.2
Permeability (mD)	0.05	0.08
s_w, unsaturated case (%)	16.9	7.3
s_w, saturated case (%)	84.3	92.4
w, unsaturated case (%)	0.6	2.4
w, saturated case (%)	3.2	30.5

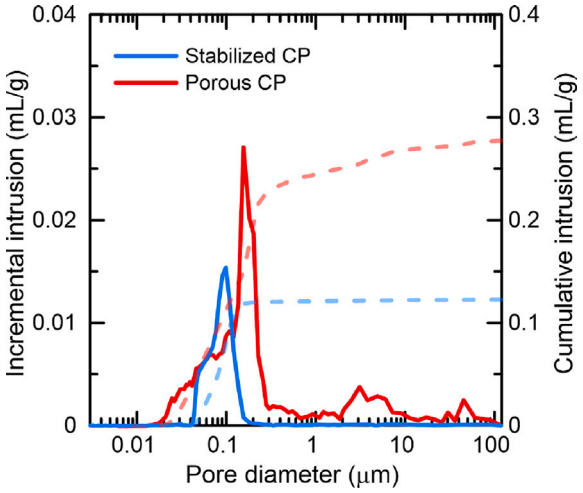

Fig. 3. Result from the mercury intrusion porosimetry test defining the relationship between the intrusion increment per pore diameter for the stabilized cement paste and porous cement paste.

pressure transducers that aid in steady-state gas flow measurements. For permeability measurements, the samples were placed in a biaxial type core holder, where 4.14 MPa (600 psi) hydrostatic pressure was applied, and after that the test procedure commenced.

A summary of the porosimetry and permeability results are provided in Table 5. The measured porosity of the porous cement paste agrees well with the empirical correlation for total porosity provided by *e.g.* Nielsen (1993), while the stabilized formulation had a considerably lower porosity. The permeability was comparable between the two samples, suggesting that the porous samples consisted of largely disconnected voids. Furthermore, from Fig. 3, it can be seen that the stabilized cement paste has a predominance of pores with a diameter between 0.04–0.2 μm. However, the porous cement paste has dual-porosity that can be defined by two intervals, the first with a pore diameter between 1–10 μm and the second between 0.02–0.3 μm. Thus, in addition to unconnected macropores, the porous cement paste presents a porosity pattern similar to that found for the stabilized cement paste.

Finally, the water content (w) and the degree of saturation (s_w) were measured for the cement paste samples used for the mechanical test program. The water content was calculated considering the ratio between the pore water mass (M_w) and the grain mass (M_s), and the degree of saturation was calculated from the ratio between the water volume (V_w) and the voids volume (V_v), the latter being estimated from the helium expansion porosimetry tests. It should be highlighted that for the evaluation of the water content and degree of saturation, the samples were dried in an oven at 105 °C so that all the water present in the sample could be eliminated and not influence the dry weight. The results found for the water content and the degree of saturation are presented in Table 5, showing that the saturated case is not 100% saturated and that the unsaturated case still has trapped and/or chemically bound water. Below, the unsaturated cement paste samples will define the reference test case in the mechanical test program, and subsequently effects of saturation and different drainage conditions will be explored.

4. Mechanical testing

The unconfined compressive strength was measured using samples with a diameter of 50 mm and a height of at least 100 mm for the unsaturated and undrained test condition (Fig. 4(a)). Subsequent triaxial tests were performed on samples of the same dimensions, using confining pressures of 10 MPa and 20 MPa. Finally, tests were also performed with saturated samples and under drained and undrained test conditions at 20 MPa confining pressure. The saturated-drained test specimens had a 38 mm diameter in order to match the available test cap diameter (Fig. 4(b)). All specimens underwent a rigorous preparation process, using self-fusing silicone tape and a heat-shrinkable FEP membrane, as presented in Fig. 4. More information about the specimen preparation and positioning process are discussed by Lima et al. (2022) and Lorenzoni et al. (2022).

The machine used for the uniaxial and triaxial mechanical tests was the MTS model 815 with a compressive load capacity of 2700 kN and a confining pressure capacity of 80 MPa, equipped with an MTS flex test 60 controller, and with two axial strain gauges and one circumferential that can be used for acquisition and also controlling the test procedure. For the unconfined compressive tests, a procedure was adopted where the circumferential displacement of the sample was fixed at a strain rate of $5{\cdot}10^{-5}$ s^{-1} until failure was detected. This control by circumferential displacement allows the acquisition of post-peak behavior of cement paste samples, as failure occurs in a controlled manner.

For the confined tests, the sample was positioned in the same way as for uniaxial compressive tests, then the triaxial cell vessel was closed and filled with Mobil Mobiltherm 605 fluid. After filling the triaxial cell, confining pressure was applied at a rate of 2 MPa/min to the preset values of 10 or 20 MPa. The subsequent test protocol was the same used for the unconfined tests, with control of circumferential displacement of the specimen. Three repeat tests were performed at each confining pressure.

Initially, tests were performed under unsaturated and undrained conditions, where any fluid existing in the pores was not allowed escape from the bulk specimen. However, as highlighted by Heukamp et al. (2001, 2003), drainage conditions during triaxial testing can affect the mechanical strength of the sample, including a lack of frictional strengthening under undrained conditions. To look for similar behavior in the current set of cement paste samples, subsequent tests were performed with saturated samples and under either drained or undrained conditions. It should be highlighted that the drained tests were performed considering the same confinement rate as the undrained tests, but half of the circumferential strain rate ($2.5{\cdot}10^{-5}$ s^{-1}). The pore pressure was not measured during the mechanical tests. Therefore, in this research, *drained* and *undrained* test conditions refer to the loading rate (slower in the case of drained tests), and the experiment configuration, *i.e.* whether a free drainage path to atmosphere exists for the pore fluid in the sample.

5. Results and discussions

5.1. Uniaxial compressive strength

As detailed above, uniaxial compression tests were performed with unsaturated samples and under undrained conditions. Here, and in the following, the rock mechanics sign convention is used, which means that compressive stresses and strains are taken as *positive*. The main unconfined test results are presented in Fig. 5, where also the average linear elastic Young's modulus has been estimated from the measurements below axial strains of 0.2%, as per (Lima et al., 2022).

As can be observed from the results shown in Fig. 5, satisfactory repeatability was achieved for both stabilized and porous cement paste

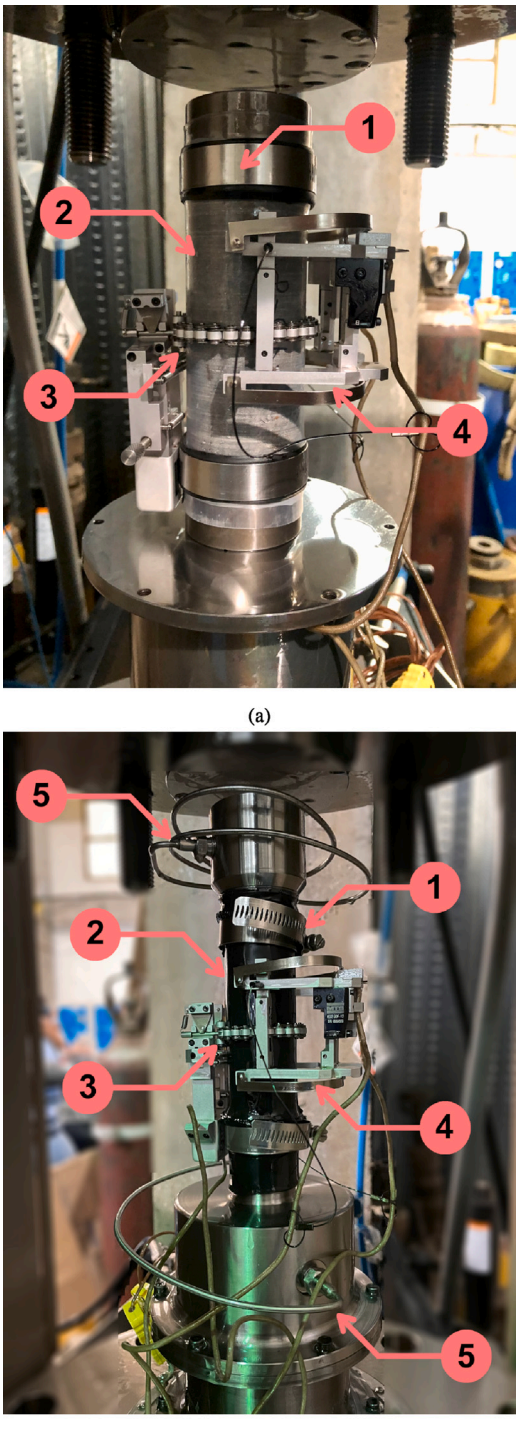

Fig. 4. Compression test setup considering the (a) undrained condition and (b) drained condition, where (1) is the cylindrical specimen with self-fusing silicone electrical tape, (2) is the heat shrinkable FEP membrane (Roll Cover-Heat Shrink® from Zeus™), and finally the specimen positioned in the MTS triaxial testing machine with the circumferential clip gauge (3), the axial LVDT (4), and for the drained test the drainage path (5).

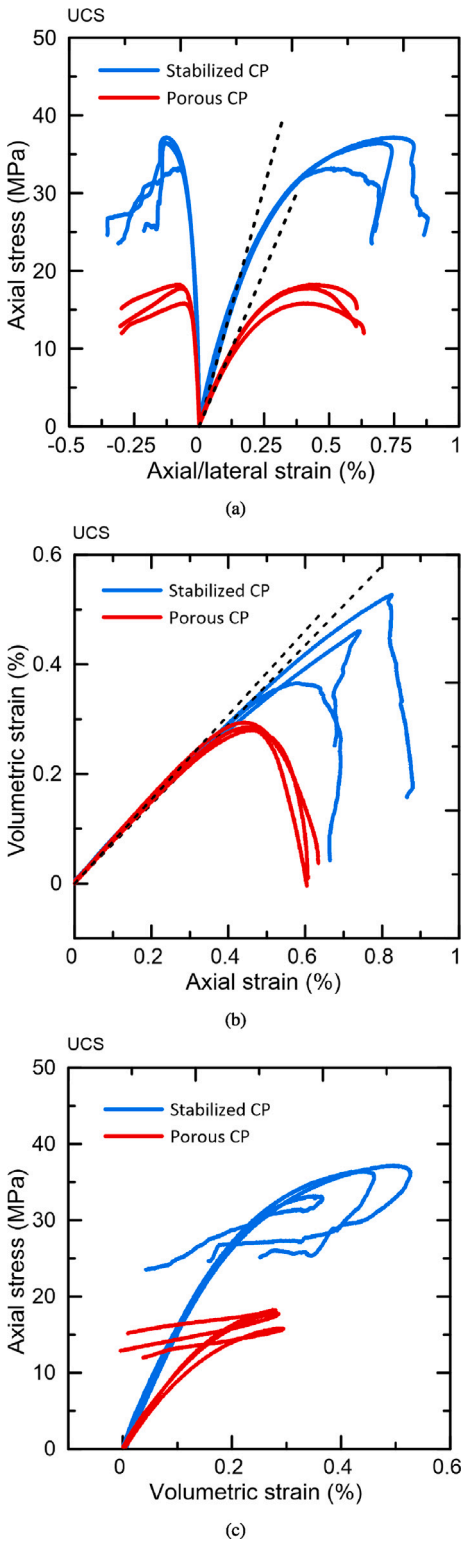

Fig. 5. Unconfined compressive test measurements for the stabilized and the porous cement paste: (a) Axial stress as function of axial strain and lateral strain; (b) Volumetric strain as function of axial strain; (c) Axial stress as function of volumetric strain.

samples. From Fig. 5(a), we observe an average Young's modulus for the stabilized samples of 12.27 ± 0.25 GPa, which was higher than that for the porous samples, which is estimated to be 8.03 ± 0.38 GPa. This range of values for cement paste Young's modulus agrees with previous measurements, *e.g.* Lima et al. (2022), Lorenzoni et al. (2022), Jimenez et al. (2019) and Li et al. (2019). A reduction in the Young's modulus with increasing porosity is also expected based on previous observations, see *e.g.* Kendall et al. (1983).

Deviations from the initial linear behavior are observed starting at an axial strain of approximately 0.2% and 0.15% for the stabilized and for the porous cement paste, respectively. The two cement pastes also differed significantly in their unconfined compressive strength, with the stabilized samples attained an average strength of 35.6 ± 2.13 MPa, and the porous cement paste about half of this value, slightly less than 17.3 ± 1.27 MPa. For all three specimens, the failure was abrupt and followed a stage of nonlinear stress–strain behavior, as seen in Fig. 5(a). In the test, it was possible to control the failure process of the material due to the controlled circumferential deformation, as discussed in Section 4.

Fig. 5(b) shows the axial strain as a function of the measured volumetric strain. Here, and in the following, the volumetric strain is defined as $\varepsilon_{vol} = \varepsilon_z + 2\varepsilon_x$, with ε_z and ε_x the axial and lateral strains, respectively. The porous cement paste showed less deformation before failure, reaching about 0.42% of axial strain and 0.28% volumetric strain, compared to 0.65% and 0.43% of the stabilized cement paste. The relatively small deformation load capacity in the absence of confinement is in agreement with previous research on cement pastes, *e.g.* Lima et al. (2022), Li et al. (2019), Thiercelin et al. (1998b,a) and Sakai et al. (2016). Also, as discussed above, the existence of larger pores and voids in the porous cement formulation results in a lower strength, as expected based on *e.g.* the Griffith fracture model (Kendall et al., 1983), and the results of Sammis and Ashby (1986), Ashby and Hallam (Née Cooksley) (1986) and Ashby and Sammis (1990). Fig. 5(b) also allows estimation of the Poisson's ratio, $\nu = -\varepsilon_x/\varepsilon_z$, since the volumetric and axial strains are related by $\varepsilon_{vol} = (1 - 2\nu)\varepsilon_z$ for elastically deforming materials. The Poisson's ratio is therefore taken as the slope of the linear curve in Fig. 5(b), corresponding to $\nu = 0.15 \pm 0.01$ for the stabilized formulation and $\nu = 0.12 \pm 0.01$ for the porous cement paste. The influence of porosity on the effective Poisson ratio is more subtle than on the Young's Modulus; previous work have shown that the Poisson's ratio may increase, decrease or remain the same with increasing porosity depending on the pore geometry and the Poisson's ratio of the matrix phase (Lutz and Zimmerman, 2021; Wang and Li, 2007; Chen et al., 2018; Stora et al., 2006).

5.2. Triaxial compressive tests

Stress–strain measurements at 10 MPa and 20 MPa confining pressure are shown in Fig. 6. The unconfined stress–strain measurements from Fig. 5(a) are included for comparison in the left panel in Fig. 6. It can be seen that even a modest confining pressure of 10 MPa increased the ductility of both stabilized and porous cement samples considerably. While the unconfined specimens failed at an axial strain ranging from 0.4% to 0.7%, a confining pressure of either 10 or 20 MPa ensures that the samples no longer lose their load-carrying capability during the test. The stabilized cement paste showed a modest frictional strengthening with increasing confining pressure and strain hardening behavior. The porous cement paste displayed considerable plastic deformation at 10 MPa confining pressure and strain hardening at 20 MPa. Similar qualitative behavior was observed recently by Lima et al. (2022) and Lorenzoni et al. (2022). The tendency toward continuous strain hardening and the lack of a clear ultimate deviatoric stress level under confining pressure is likely linked to compaction and pore closure within the samples, (Nelson and Guillot, 2006).

Post-test images of the stabilized and porous cement paste samples are provided in Fig. 7. Both sample types exhibited well-defined failure planes at unconfined test conditions, with either predominantly axial failure planes for the stabilized cement samples and an inclined shear failure plane for the porous samples. No obvious shear failure planes were observed in stabilized samples tested with confining pressure, but several smaller shear planes was seen in the porous cement paste samples.

A summary of the measured elastic moduli is provided in Table 6, including Young's modulus, E, Poisson's ratio, ν and the bulk modulus, K. We observe that the elastic moduli for the porous cement paste exhibit a greater sensitivity to confining pressure and a greater relative reduction with confining pressure compared to that of the stabilized formulation. Moreover, it should be highlighted that the elastic moduli decrease with increasing confining pressure for both cement paste formulations.

Table 6
Summary of elastic properties of specimens subjected to unconfined and confined compression test.

Formulation	Confining pressure	E (GPa)	ν	K (GPa)
Stabilized CP	0 MPa	12.27 ± 0.25	0.15 ± 0.01	5.84 ± 0.09
	10 MPa	12.08 ± 0.52	0.12 ± 0.01	5.30 ± 0.18
	20 MPa	10.34 ± 0.19	0.10 ± 0.01	4.31 ± 0.06
Porous CP	0 MPa	8.03 ± 0.38	0.12 ± 0.01	3.52 ± 0.13
	10 MPa	5.95 ± 0.51	0.05 ± 0.01	2.20 ± 0.17
	20 MPa	4.24 ± 0.08	0.03 ± 0.01	1.50 ± 0.03

The volumetric strain measured during the triaxial tests is shown in Fig. 8. The relatively compliant porous cement paste displayed considerable volumetric deformation under confined conditions and a volumetric strain that was nearly equal to the measured axial strain induced in the sample. This is also reflected in the relatively small value of Poisson's ratio listed in Table 6 for the confined porous cement paste. Finally, the deviatoric stress is plotted as function of volumetric strain for the two formulations in Fig. 9. As seen from the Figure, the two formulations exhibited very similar volumetric strain response at both levels of confining pressure.

As observed above, a marked impact of the confining pressure is to enable the cement samples to withstand considerable volumetric deformation under strain hardening. A certain frictional strengthening is observed with increasing confining pressure, but the more important effect of confinement is to support ductile deformation, as previously observed by Lima et al. (2022). We attribute the volumetric deformation observed in Figs. 8 and 9 mainly to a gradual closure of pores and a reduced porosity. Since the matrix does not collapse, the increased degree of compaction results in strain hardening and the absence of any well-defined peak strength or loss of load-bearing capability, (Nelson and Guillot, 2006). A visual interpretation of this mechanism is provided in Fig. 10.

5.3. The effect of saturation and drainage to the triaxial stress state behavior

In addition to porosity, the sample saturation and test conditions can impact the mechanical behavior of hardened cement pastes. It is generally considered that saturated cement pastes have lower mechanical strength compared to their dry counterparts, since the presence of water can favor initiation and the spread of cracks through the sample, (Taylor, 1997). Further, sensitivity to drainage conditions can be observed in triaxial testing of weakened and highly porous cements. This is considered to be due to the relatively compliant matrix of weakened cement, which means that undrained cement samples will experience high pore pressure and low effective confining stresses under confinement, (Heukamp et al., 2001). To explore such mechanisms within the current cement formulations, a suite of drained and undrained triaxial tests were performed at a confining pressure of 20 MPa.

Fig. 11 shows the behavior of the stabilized cement paste under the three different test conditions of this study: Unsaturated and undrained ("reference") and saturated samples under undrained or drained conditions. One can observe that the saturated and undrained test samples in fact fail at an axial strain of 0.5% and at an axial stress of approximately 38 MPa. This behavior is very similar to the *unconfined* behavior of this cement paste formulation, as shown in Fig. 5(a). In effect, the saturation and the trapping of this fluid during testing is effectively removing

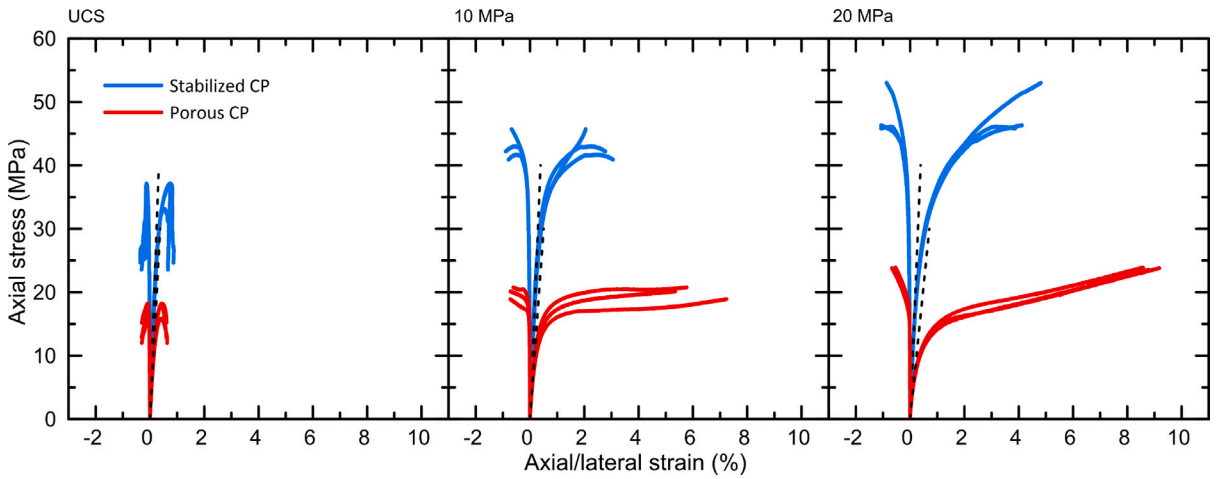

Fig. 6. Measurements of axial and lateral strains for increasing deviatoric stresses at unconfined conditions (UCS) and at two different confining pressures.

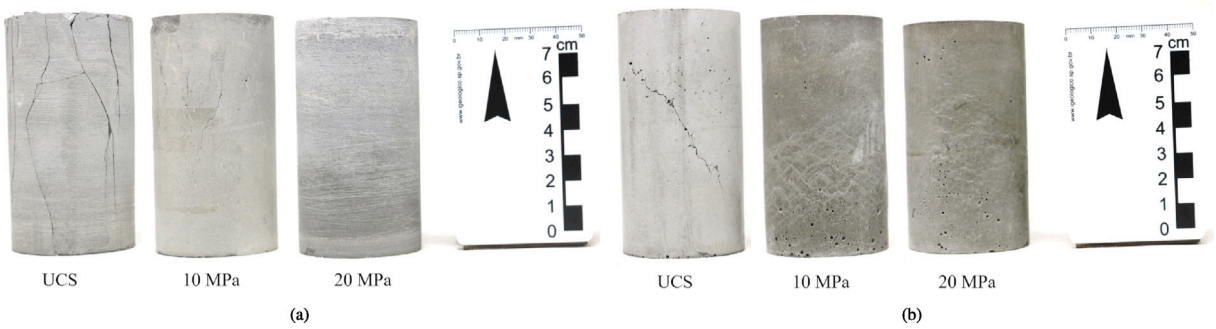

Fig. 7. Specimens failure modes when under unconfined and confined compression tests: (a) Stabilized CP specimens and (b) Porous CP specimens.

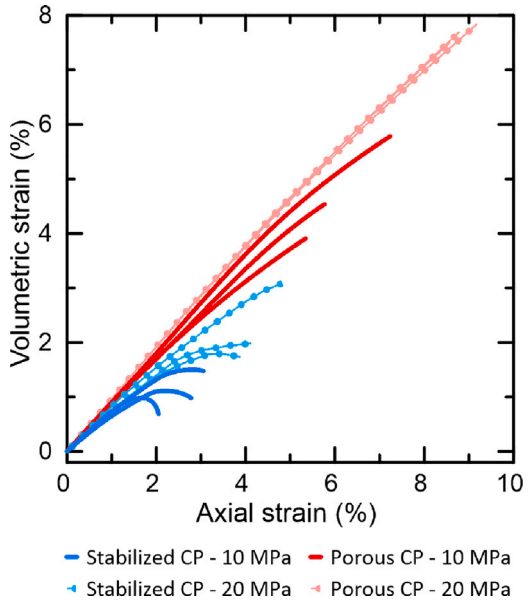

Fig. 8. Axial and volumetric strains measured at different confining pressures and for the two different cement pastes. The volumetric strain is measured relative to the start of the deviatoric loading phase.

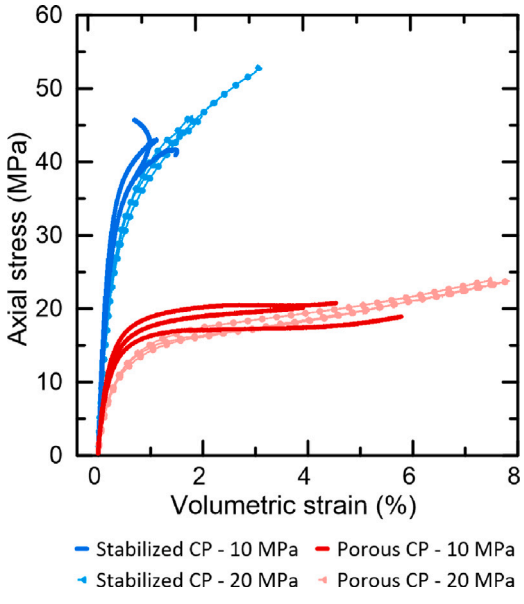

Fig. 9. Volumetric strain by means of axial stress for samples tested under different confining pressures and for the two different cement pastes. Note that the volumetric strain is here measured relative to the start of the deviatoric loading phase.

the strengthening effect of the confining pressure. We interpret the result as per Heukamp et al. (2001), *i.e.* the saturated and *undrained* test condition reduces the effective confining stress in the sample and the net triaxial behavior of the cement paste is very similar to its unconfined behavior. This confining stress reduction was also observed by Meng et al. (2021), who modeled the transient thermoporoelastic effects related to the wellbore conditions. Moreover, although the samples are not 100% saturated, the low permeability provides localized

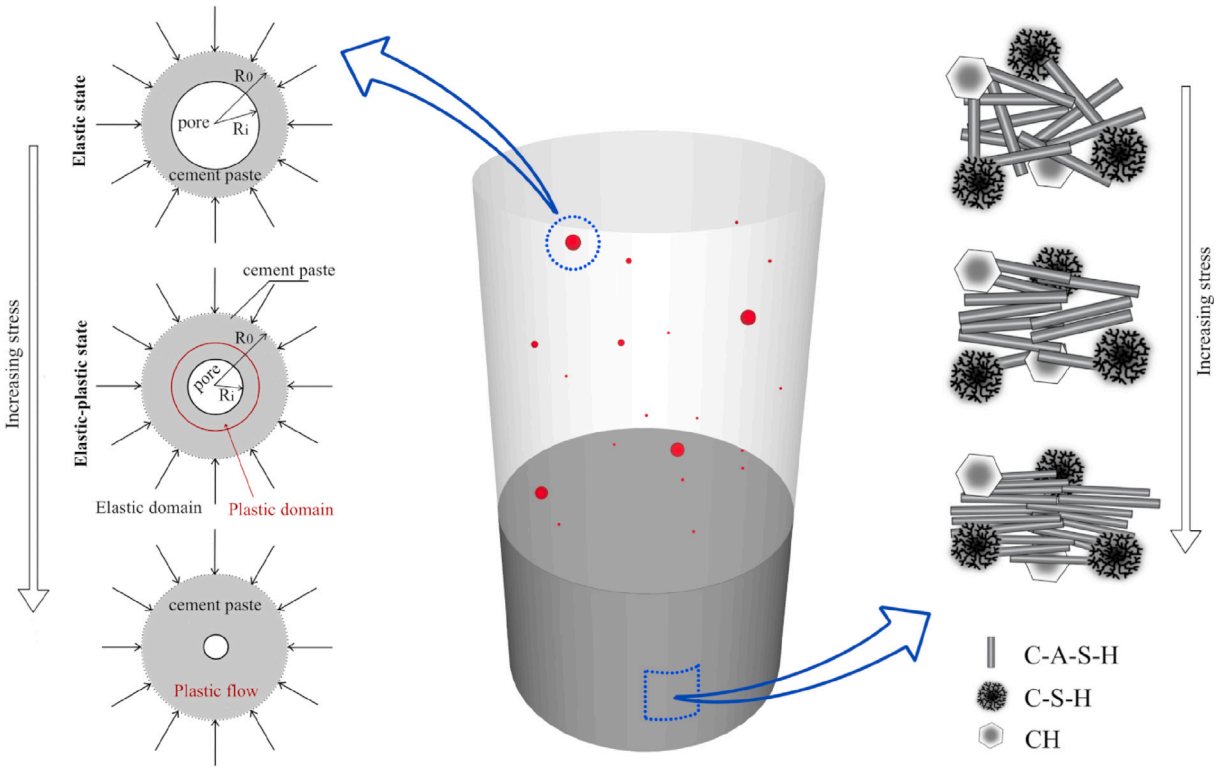

Fig. 10. Mechanisms involved in the behavior of cement pastes when subjected to triaxial loads with constant confining pressure.

pore pressure concentrations that generate the material failure process and result in the aforementioned behavior.

Turning to the drained test condition, similar stress–strain behavior is observed as the reference case, *i.e. unsaturated* and *undrained*. The loading is likely slow enough to allow the drained test specimens to bleed off significant pore pressure, resulting in effective confining stresses in the sample and ductile behavior. However, as is evident in Fig. 11(b), the saturated sample is stiffer than the unsaturated reference sample, resulting in slightly larger elastic moduli than the reference. This apparent stiffening of the structure is in accordance with previous observations, (Taylor, 1997).

The corresponding reference and saturated sample test results for the porous cement paste formulation are shown in Fig. 12. The results suggest less sensitivity to the drainage conditions in this case, with none of the samples failing during the loading cycle, and relatively similar stress and strain relations. One can observe from Figs. 12(a) and 12(c) that the two saturated samples exhibit a slightly increased stiffening during the strain hardening phase compared to the reference measurements; this can be observed as an increase in axial stress at a certain fixed axial or volumetric strain. The relation between axial and volumetric strains is nearly independent of drainage conditions, as seen in Fig. 12(b), suggesting that also the saturated samples are characterized by a very low value of Poisson's ratio as per the reference case.

For both cement formulations, we observe a mechanical stiffening effect compared to the reference case when the sample is saturated and tested under drained conditions. Combining the relatively slow loading rate and the drained test condition make these saturated samples mechanically stiffer than the reference (unsaturated) counterpart. The main difference between the stabilized and the porous cement formulation in terms of their saturated behavior, is seen for the undrained test condition. While the stabilized cement formulation behaved almost as it was unconfined, the porous formulation maintains its ductility and strain hardening characteristics under undrained conditions. A bit surprisingly, these samples exhibit an intermediate stiffness compared to the reference and the saturated, drained tests with the porous cement paste. A possible explanation for this behavior is that the porous cement samples develop small cracks and micro-fractures as a consequence of trapped pore fluid and the undrained test conditions. While these small defects do not cause macroscopic failure of the samples, they may impart a slight softening of the material.

Finally, a summary of the elastic moduli for the different drainage and saturation conditions is provided in Table 7. As indicated above, saturating the stabilized cement samples and trapping the fluid during the test, results in a significant mechanical stiffening, as seen in the elastic moduli. This observation is in accordance with general expectations (Taylor, 1997). The saturated and undrained elastic moduli for the stabilized cement paste are in fact similar to those found by Lima et al. (2022) for three year old oil well cement samples in their unsaturated state. The porous cement pastes show generally less sensitivity to saturation and drainage conditions, which is at first surprising since one may expect the more porous structure to impart a more pronounced sensitivity to the test conditions. As indicated above, it is perceived that the emergence of small defects and micro-cracks renders the structure effectively softer under undrained conditions compared to drained conditions for this specific cement composition. For the Poisson's ratio in particular, Carcione and Cavallini (2002) showed that dry material samples tend to have significantly smaller values of the ratio compared to saturated samples. On the other hand, specimens containing mainly round voids, that are stiff pores, do not show major variations in ν with effective stress (Carcione and Cavallini, 2002; Tatham, 1982; Todd and Simmons, 1972). Therefore, for the case of the porous cement paste, the random distribution of rounded macropores may be influencing the values of Poisson's ratio found, since all three test conditions resulted in the same, low value of $\nu = 0.03$.

5.4. Current study limitations and uncertainty

The curing conditions of the class G cement paste specimens used for the above measurements did not follow defined schedules to simulate

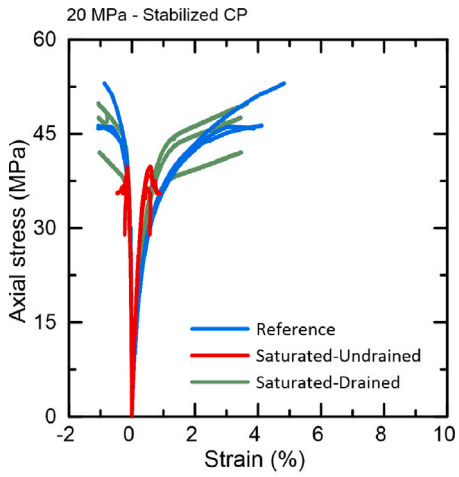

(a)

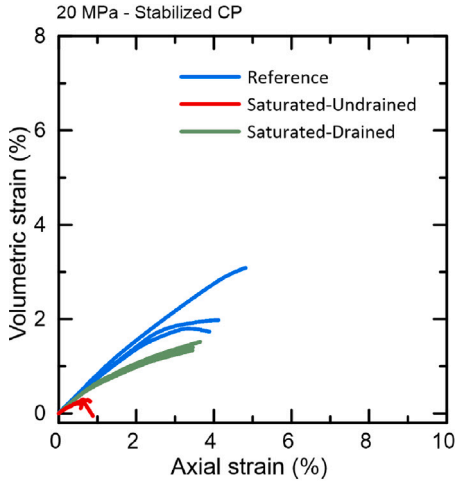

(b)

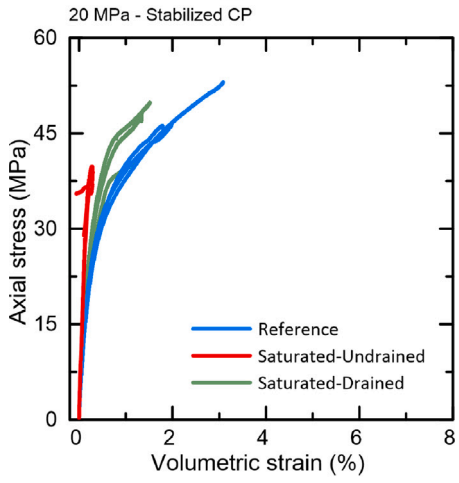

(c)

Fig. 11. Confined compression behavior for the stabilized cement paste under different saturation and drainage conditions, with the reference measurements corresponding to unsaturated and undrained conditions. (a) Axial stress as function of axial and lateral strain, (b) volumetric strain as function of axial strain, and (c) axial stress as function of volumetric strain response.

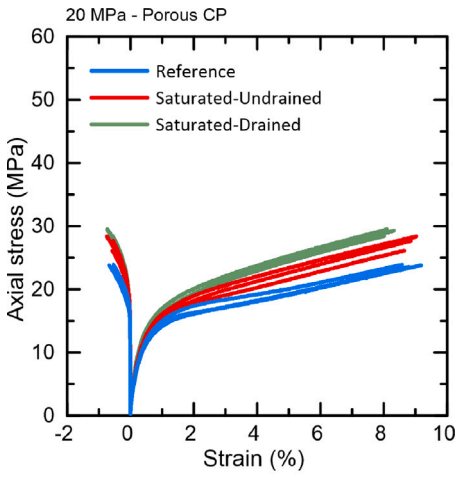

(a)

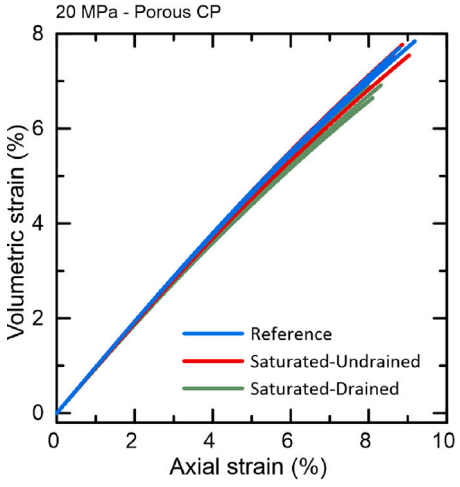

(b)

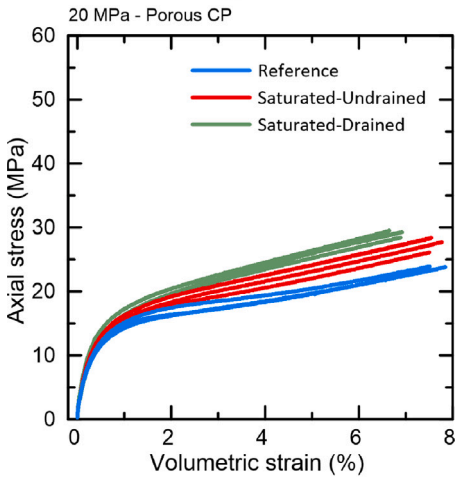

(c)

Fig. 12. Confined compression behavior for the porous cement paste under different saturation and drainage conditions, with the reference measurements corresponding to unsaturated and undrained conditions. (a) Axial stress as function of axial and lateral strain, (b) volumetric strain as function of axial strain, and (c) axial stress as function of volumetric strain response.

downhole conditions, and the mechanical tests were performed at room temperature. In addition, the molding process followed the recommendations of API 10A and API 10B but did not take into account the possible existence of drilling fluids and spacer fluids as occurs in field applications. In this way, the curing and molding conditions may have affected the mechanical properties of the specimens tested in this study

Table 7
Summary of elastic properties of specimens subjected to a saturated condition compared to the reference case.

Formulation	Confining pressure	Test condition	E (GPa)	ν	K (GPa)
Stabilized CP	20 MPa	Reference	10.34 ± 0.19	0.10 ± 0.01	4.31 ± 0.08
		Saturated, drained	10.83 ± 0.68	0.13 ± 0.01	4.88 ± 0.28
		Saturated, undrained	14.00 ± 0.15	0.19 ± 0.01	7.56 ± 0.06
Porous CP	20 MPa	Reference	4.24 ± 0.09	0.03 ± 0.01	1.50 ± 0.23
		Saturated, drained	4.50 ± 0.58	0.03 ± 0.01	1.60 ± 0.24
		Saturated, undrained	4.50 ± 0.07	0.03 ± 0.01	1.60 ± 0.03

and caused the quantitative stress–strain curves presented above to be different from the real downhole behavior of the same cement system. Moreover, one more limitation could be that the cement is not tested under fully in situ conditions, without depressurization and cooling. In addition, the saturation procedure was carried out using a vacuum chamber with a maximum pressure of 760 Torrs, and no constant measurement of Skempton's coefficient (B) to ensure full saturation was performed. Therefore, as seen in the section on the initial cement paste characterization, the saturation degree of the samples in the saturated test condition did not reach 100%. Finally, as the pore pressure was not acquired in the saturated tests, there is a limitation in estimating the effective stress of the specimens tested. Further, as it is also uncertain how the pore pressure evolved over the course of the loading, the drained test conditions in our experiments may not represent *fully* drained conditions. We consider these as the most relevant sources of uncertainty when comparing the results presented in this study and the real downhole behavior and when defining the influence of saturation on the mechanical behavior of class G cement paste specimens.

6. Summary and conclusions

The mechanical behavior of two class G cement paste formulations for oil wells was studied, focusing on the effect of porosity, saturation and drainage condition. The initial characterization of the samples using mass density, porosimetry, and permeability measurements showed significant variations in the microstructure of the two cement pastes, defining a stabilized cement paste with an average porosity of 7% and a porous cement paste with 41%.

Unconfined cement paste specimens show linear behavior up to about 0.2% with an average Young's modulus of 12.27 GPa and 8.03 GPa and Poisson's ratio of 0.15 and 0.12 for the stabilized and porous case, respectively. At higher strains, the stress–strain response becomes nonlinear, ending up with a brittle failure at axial strains of approximately 0.5%. The corresponding average uniaxial compressive strength is 36 MPa for the stabilized sample and 18 MPa for the porous sample.

As expected, the confining pressure gave the samples a behavior markedly different from the uniaxial case, implying considerable volumetric deformation support under strain hardening for both evaluated formulations. However, this behavior was more significant for the porous sample. Although some frictional reinforcement is observed, the most important effect of confinement is to support ductile deformation. This significant volumetric deformation was attributed to a gradual closing of the pores and a reduced porosity. As the matrix does not collapse, increasing the degree of compaction results in the absence of any well-defined peak strength or loss of load-bearing capacity. Furthermore, increasing confining pressure also reduces Young's modulus and Poisson ratio of the cement paste, suggesting an effectively smoother response to higher confining pressure.

Finally, the behavior of the two cement pastes formulations when under saturation conditions were different. Saturating the stabilized cement samples and retaining the fluid during the test results in significant mechanical stiffening, as seen in the elastic moduli. Furthermore, the non-drainage of the fluid in the stabilized sample may have caused pore pressure to build up, which resulted in a stress–strain behavior similar to the unconfined case. On the other hand, porous cement pastes showed less sensitivity to saturation and drainage conditions, which, due to the appearance of small defects and microcracks, make the structure effectively softer, even in undrained conditions.

CRediT authorship contribution statement

Victor Nogueira Lima: Conceptualization, Methodology, Investigation, Writing – original draft, Writing – review & editing. **Hans Joakim Skadsem:** Conceptualization, Supervision, Writing – original draft. **Katherine Beltrán-Jiménez:** Methodology, Investigation. **Alexandr Zhemchuzhnikov:** Investigation, Writing – original draft. **Raquel Quadros Velloso:** Resources, Supervision. **Flávio de Andrade Silva:** Resources, Supervision.

Declaration of competing interest

The authors declare that they have no known competing financial interests or personal relationships that could have appeared to influence the work reported in this paper.

Data availability

Data will be made available on request.

Acknowledgments

This study was financed in part by the Coordenação de Aperfeiçoamento de Pessoal de Nível Superior – Brasil (CAPES) – Finance Code 001, by Brazilian funding agencies FAPERJ and CNPq, by Lafarge Holcim, with the donation of class G cement, by BASF, with the donation of the defoamer, and by Kuraray, with the donation of the Kuraray Poval™ additive. The production of this article is a research cooperation between PUC-Rio, NORCE and UiS funded by the Research Council of Norway (RCN) under the BRANOR Project (30929).

References

Ahmed, H.S., 2022. New approach of mercury intrusion porosimetry to evaluate the microstructure of cement-bases matrixes: Application on slag cement mortars. Mater. Today: Proc. http://dx.doi.org/10.1016/J.MATPR.2022.02.233.

API, 2011. API 10a: Specification for cements and materials for well cementing.

API, 2013. 10B-2: Recommended practice for testing well cements.

Ashby, M.F., Hallam (Née Cooksley), S.D., 1986. The failure of brittle solids containing small cracks under compressive stress states. Acta Metall. 34, 497–510. http://dx.doi.org/10.1016/0001-6160(86)90086-6.

Ashby, M.F., Sammis, C.G., 1990. The damage mechanics of brittle solids in compression. Pure Appl. Geophys. 133, 489–521. http://dx.doi.org/10.1007/BF00878002.

Balshin, M.Y., 1949. Relation of mechanical properties of powder metals and their porosity and the ultimate properties of porous metal–ceramic materials. In: Dokl Akad Nauk SSSR. pp. 831–834.

Bois, A.P.P., Garnier, A., Rodot, F., Saint-Marc, J., Aimard, N., 2011. How to prevent loss of zonal isolation through a comprehensive analysis of microannulus formation. SPE Drill. Complet. 26, 13–31. http://dx.doi.org/10.2118/124719-PA.

Brouwers, H., 2004. The work of powers and brownyard revisited: Part 1. Cem. Concr. Res. 34, 1697–1716. http://dx.doi.org/10.1016/j.cemconres.2004.05.031, h. F. W. Taylor Commemorative Issue.

Carcione, J.M., Cavallini, F., 2002. Poisson's ratio at high pore pressure. Geophys. Prospect. 50, 97–106. http://dx.doi.org/10.1046/J.1365-2478.2002.00299.X.

Chen, H., Xu, B., Mo, Y.L., Zhou, T., 2018. Behavior of meso-scale heterogeneous concrete under uniaxial tensile and compressive loadings. Constr. Build. Mater. 178, 418–431. http://dx.doi.org/10.1016/J.CONBUILDMAT.2018.05.052.

Chindaprasirt, P., Hatanaka, S., Chareerat, T., Mishima, N., Yuasa, Y., 2008. Cement paste characteristics and porous concrete properties. Constr. Build. Mater. 22, 894–901. http://dx.doi.org/10.1016/j.conbuildmat.2006.12.007.

Contrafatto, L., Cuomo, M., Gazzo, S., 2016. A concrete homogenisation technique at meso-scale level accounting for damaging behaviour of cement paste and aggregates. Comput. Struct. 173, 1–18. http://dx.doi.org/10.1016/J.COMPSTRUC.2016.05.009.

Cunningham, E., Heathman, J., Kutchko, B., Benge, G., Maxson, J., DeBruijn, G., Buford, C., 2017. Defining the difference between laboratory and field-generated foamed cement. In: OTC Offshore Technology Conference. pp. 1–48. http://dx.doi.org/10.4043/27581-MS, OTC-27581-MS.

de Roziéres, J., Ferriére, R., 1991. Foamed-cement characterization under downhole conditions and its impact on job design. SPE Prod. Eng. 6, 297–304. http://dx.doi.org/10.2118/19935-PA.

Fassin, M., Eggersmann, R., Wulfinghoff, S., Reese, S., 2019. Gradient-extended anisotropic brittle damage modeling using a second order damage tensor – Theory, implementation and numerical examples. Int. J. Solids Struct. 167, 93–126. http://dx.doi.org/10.1016/J.IJSOLSTR.2019.02.009.

Ghabezloo, S., Sulem, J., Guéon, F., Saint-Marc, J., 2008. Poromechanical behaviour of hardened cement paste under isotropic loading. Cem. Concr. Res. 38, 1424–1437. http://dx.doi.org/10.1016/J.CEMCONRES.2008.06.007, https://www.sciencedirect.com/science/article/pii/S0008884608001439.

Griffith, A.A., 1921. The phenomena of rupture and flow in solids. Trans. R. Soc. Lond. A 221, 163–198.

Handin, J., 1965. Strength of oil well cements at downhole pressure-temperature conditions. SPE J. 5, 341–347. http://dx.doi.org/10.2118/1300-PA.

Hasselman, D.P.H., 1963. Relation between effects of porosity on strength and on Young's modulus of elasticity of polycrystalline materials. J. Am. Ceram. Soc. 46, 564–565. http://dx.doi.org/10.1111/j.1151-2916.1963.tb14615.x.

He, T., Wang, T., Xie, D., Daemen, J.J., 2022. The mechanism of pores enhancing the deformation of completion cement under confining pressure. Cem. Concr. Compos. 125, 104322. http://dx.doi.org/10.1016/J.CEMCONCOMP.2021.104322.

Hedenblad, G., 1997. The use of mercury intrusion porosimetry or helium porosity to predict the moisture transport properties of hardened cement paste. Adv. Cem. Based Mater. 6, 123–129. http://dx.doi.org/10.1016/S1065-7355(97)90019-5.

Heukamp, F., Ulm, F.J., Germaine, J., 2001. Mechanical properties of calcium-leached cement pastes: Triaxial stress states and the influence of the pore pressures. Cem. Concr. Res. 31, 767–774. http://dx.doi.org/10.1016/S0008-8846(01)00472-0.

Heukamp, F.H., Ulm, F.J., Germaine, J.T., 2003. Poroplastic properties of calcium-leached cement-based materials. Cem. Concr. Res. 33, 1155–1173. http://dx.doi.org/10.1016/S0008-8846(03)00024-3.

Hewlett, P. (Ed.), 2003. Lea's Chemistry of Cement and Concrete. Elsevier.

Irico, S., Qvaeschning, D., Mutke, S., Deuse, T., Gastaldi, D., Canonico, F., 2021. Durability of high performance self-compacting concrete with granulometrically optimized slag cement. Constr. Build. Mater. 298, 123836. http://dx.doi.org/10.1016/J.CONBUILDMAT.2021.123836.

Jennings, H.M., Thomas, J.J., Rothstein, D., Chen, J.J., 2002. Cements As Porous Materials. John Wiley & Sons, Ltd., pp. 2971–3028. http://dx.doi.org/10.1002/9783527618286.ch40, chapter 6.11.

Jimenez, W.C., Darbe, R., Pang, X., 2019. Enhanced mechanical-integrity characterization of oilwell annular sealants under in-situ downhole conditions. SPE J. 24, 2308–2319. http://dx.doi.org/10.2118/185341-PA.

Kendall, K., Howard, A.J., Birchall, J.D., Pratt, P.L., Proctor, B.A., Jefferis, S.A., Hirsch, P.B., Birchall, J.D., Double, D.D., Kelly, A., Moir, G.K., Pomeroy, C.D., 1983. The relation between porosity, microstructure and strength, and the approach to advanced cement-based materials. Phil. Trans. R. Soc. Lond. Ser A, Math. Phys. Sci. 310, 139–153. http://dx.doi.org/10.1098/rsta.1983.0073.

Krus, M., Hansen, K.K., Küzel, H.M., 1997. Porosity and liquid absorption of cement paste. Mater. Struct. 30 (7), 394–398. http://dx.doi.org/10.1007/BF02498561, 1997 30. https://link.springer.com/article/10.1007/BF02498561.

Li, Y., Lu, Y., Ahmed, R., Han, B., Jin, Y., 2019. Nonlinear stress-strain model for confined well cement. http://dx.doi.org/10.3390/ma12162626.

Lian, C., Zhuge, Y., Beecham, S., 2011. The relationship between porosity and strength for porous concrete. Constr. Build. Mater. 25, 4294–4298. http://dx.doi.org/10.1016/j.conbuildmat.2011.05.005.

Lima, V.N., Silva, F.d.A., Skadsem, H.J., Beltrá-Jiménez, K., Sunde, J.K., 2022. Effects of confinement pressure on the mechanical behavior of an oil well cement paste. J. Pet. Sci. Eng. 208, 109769. http://dx.doi.org/10.1016/J.PETROL.2021.109769.

Liu, L., Qin, S., Wang, X., 2018. Poro-elastic–plastic model for cement-based materials subjected to freeze–thaw cycles. Constr. Build. Mater. 184, 87–99. http://dx.doi.org/10.1016/J.CONBUILDMAT.2018.06.197.

Lorenzoni, R., Lima, V.N., Figueiredo, T.C.S., Hering, M., Paciornik, S., Curbach, M., Mechtcherine, V., Silva, F.de.Andrade., 2022. Macro and meso analysis of cement-based materials subjected to triaxial and uniaxial loading using X-ray microtomography and digital volume correlation. Constr. Build. Mater. 323, 126558. http://dx.doi.org/10.1016/J.CONBUILDMAT.2022.126558, URL: https://linkinghub.elsevier.com/retrieve/pii/S0950061822002501.

Lutz, M.P., Zimmerman, R.W., 2021. The effect of pore shape on the Poisson ratio of porous materials. Math. Mech. Solids 26, 1191–1203. http://dx.doi.org/10.1177/10812865211023535.

Malecot, Y., Zingg, L., Briffaut, M., Baroth, J., 2019. Influence of free water on concrete triaxial behavior: The effect of porosity. Cem. Concr. Res. 120, 207–216. http://dx.doi.org/10.1016/j.cemconres.2019.03.010.

Meng, M., Frash, L., Carey, J.W., Niu, Z., Zhang, W., Guy, N., Lei, Z., Li, W., Welch, N., 2021. Predicting cement-sheath integrity with consideration of initial state of stress and thermoporoelastic effects. SPE J. 26, 3505–3528. http://dx.doi.org/10.2118/205344-PA.

Mindess, S., 1970. Relation between the compressive strength and porosity of autoclaved calcium silicate hydrates. J. Am. Ceram. Soc. 53, 621–624. http://dx.doi.org/10.1111/j.1151-2916.1970.tb15986.x.

Nelson, E.B., Guillot, D. (Eds.), 2006. Well Cementing, second ed Schlumberger, Sugar Land, Texas, US.

Nielsen, L.F., 1993. Strength development in hardened cement paste: examination of some empirical equations. Mater. Struct. 26, 255–260. http://dx.doi.org/10.1007/BF02472946.

Odler, I., Rößler, M., 1985. Investigations on the relationship between porosity, structure and strength of hydrated portland cement pastes. II. Effect of pore structure and of degree of hydration. Cem. Concr. Res. 15, 401–410. http://dx.doi.org/10.1016/0008-8846(85)90113-9, https://www.sciencedirect.com/science/article/pii/0008884685901139.

Pavía, S., Condren, E., 2008. Study of the durability of OPC versus GGBS Concrete on Exposure to Silage Effluent. J. Mater. Civ. Eng. 20, 313–320. http://dx.doi.org/10.1061/(ASCE)0899-1561(2008)20:4(313), https://ascelibrary.org/doi/abs/10.1061/%28ASCE%290899-1561%282008%2920%3A4%28313%29.

Rashad, A.M., 2018. An overview on rheology, mechanical properties and durability of high-volume slag used as a cement replacement in paste, mortar and concrete. Constr. Build. Mater. 187, 89–117. http://dx.doi.org/10.1016/J.CONBUILDMAT.2018.07.150.

Roy, D.M., Gouda, G.R., 1973. Porosity-strength relation in cementitious materials with very high strengths. J. Am. Ceram. Soc. 56, 549–550. http://dx.doi.org/10.1111/j.1151-2916.1973.tb12410.x.

Ryshkewitch, E., 1953. Compression strength of porous sintered alumina and zirconia. J. Am. Ceram. Soc. 36, 65–68. http://dx.doi.org/10.1111/j.1151-2916.1953.tb12837.x.

Sakai, Y., Nakatani, M., Takeuchi, A., Omorai, Y., Kishii, T., 2016. Mechanical behavior of cement paste and alterations of hydrates under high-pressure triaxial testing. J. Adv. Concr. Technol. 14, 1–12. http://dx.doi.org/10.3151/jact.14.1.

Sammis, C.G., Ashby, M.F., 1986. The failure of brittle porous solids under compressive stress states. Acta Metall. 34, 511–526. http://dx.doi.org/10.1016/0001-6160(86)90087-8.

Schiller, K., 1971. Strength of porous materials. Cem. Concr. Res. 1, 419–422. http://dx.doi.org/10.1016/0008-8846(71)90035-4.

Stora, E., He, Q.C., Bary, B., 2006. Influence of inclusion shapes on the effective linear elastic properties of hardened cement pastes. Cem. Concr. Res. 36, 1330–1344. http://dx.doi.org/10.1016/J.CEMCONRES.2006.02.007.

Tatham, R.H., 1982. Vp/Vs and lithology. Geophysics 47, 336–344. http://dx.doi.org/10.1190/1.1441339.

Taylor, H., 1997. Cement Chemistry, 2nd ed Thomas Telford Publishing., http://dx.doi.org/10.1680/cc.25929.

Thiercelin, M., Baumgarte, C., Guillot, D., 1998a.. A soil mechanics approach to predict cement sheath behavior. In: SPE/ISRM Rock Mechanics in Petroleum Engineering. pp. 329–337. http://dx.doi.org/10.2118/47375-MS, SPE/ISRM 47375.

Thiercelin, M.J., Dargaud, B., Baret, J.F., Rodriquez, W.J., 1998b. Cement design based on cement mechanical response. SPE Drill. Complet. 13, 266–273. http://dx.doi.org/10.2118/52890-PA.

Todd, T., Simmons, G., 1972. Effect of pore pressure on the velocity of compressional waves in low-porosity rocks. J. Geophys. Res. 77 (1896–1977), 3731–3743. http://dx.doi.org/10.1029/JB077i020p03731.

Ulm, F.J., Constantinides, G., Heukamp, F.H., 2004. Is concrete a poromechanics material? - A multiscale investigation of poroelastic properties. Mat. Struct. 37, 43–58. http://dx.doi.org/10.1007/BF02481626.

Vu, X.D., Briffaut, M., Malecot, Y., Daudeville, L., Ciree, B., 2015. Influence of the saturation ratio on concrete behavior under triaxial compressive loading. Sci. Technol. Nucl. Installations 2015, 1–10. http://dx.doi.org/10.1155/2015/976387.

Wang, H., Li, Q., 2007. Prediction of elastic modulus and Poisson's ratio for unsaturated concrete. Int. J. Solids Struct. 44, 1370–1379. http://dx.doi.org/10.1016/J.IJSOLSTR.2006.06.028.

Yudenfreund, M., Hanna, K.M., Skalny, J., Older, I., Brunauer, S., 1972. Hardened portland cement pastes of low porosity V. Compressive Strength. Cement Concr. Res. 2, 731–743. http://dx.doi.org/10.1016/0008-8846(72)90008-7.

Yurtdas, I., Xie, S., Burlion, N., Shao, J., Saint-Marc, J., Garnier, A., 2011. Influence of chemical degradation on mechanical behavior of a petroleum cement paste. Cem. Concr. Res. 41, 412–421. http://dx.doi.org/10.1016/j.cemconres.2011.01.008.

Zingg, L., Briffaut, M., Baroth, J., Malecot, Y., 2016. Influence of cement matrix porosity on the triaxial behaviour of concrete. Cem. Concr. Res. 80, 52–59. http://dx.doi.org/10.1016/j.cemconres.2015.10.005.